

Using Spatio-temporal Deep Learning for Forecasting Demand and Supply-demand Gap in Ride-hailing System with Anonymized Spatial Adjacency Information

Md. Hishamur Rahman^{1*}, Shakil Mohammad Rifaat²

¹ Department of Civil Engineering, International University of Business Agriculture and Technology, Dhaka, Bangladesh

² Department of Civil and Environmental Engineering, Islamic University of Technology, Gazipur, Bangladesh

[*hishamur@iubat.edu](mailto:hishamur@iubat.edu)

Abstract: To reduce passenger waiting time and driver search friction, ride-hailing companies need to accurately forecast spatio-temporal demand and supply-demand gap. However, due to spatio-temporal dependencies pertaining to demand and supply-demand gap in a ride-hailing system, making accurate forecasts for both demand and supply-demand gap is a difficult task. Furthermore, due to confidentiality and privacy issues, ride-hailing data are sometimes released to the researchers by removing spatial adjacency information of the zones, which hinders the detection of spatio-temporal dependencies. To that end, a novel spatio-temporal deep learning architecture is proposed in this paper for forecasting demand and supply-demand gap in a ride-hailing system with anonymized spatial adjacency information, which integrates feature importance layer with a spatio-temporal deep learning architecture containing one-dimensional convolutional neural network (CNN) and zone-distributed independently recurrent neural network (IndRNN). The developed architecture is tested with real-world datasets of Didi Chuxing, which shows that our models based on the proposed architecture can outperform conventional time-series models (e.g., ARIMA) and machine learning models (e.g., gradient boosting machine, distributed random forest, generalized linear model, artificial neural network). Additionally, the feature importance layer provides an interpretation of the model by revealing the contribution of the input features utilized in prediction.

Keywords: Demand, Supply-demand gap, Deep learning, Convolutional neural network, Recurrent neural network

1. Introduction

Ride-hailing is recognized as a disruptive urban transportation mode where registered private car owners provide on-demand rides by driving their vehicles [1]. With the advancement of mobile technologies, ride-hailing services are replacing conventional taxi services and reshaping the mode choice behaviour of passengers. In the last few years, several ride-hailing companies such as Uber, Lyft, Didi have gained increasing popularity in many cities around the world. A recent study found that around 20% of adults in an urban area are using ride-hailing services [2]. Ride-hailing services are conducted through mobile applications, which coordinate the matching of passengers' requests with vacant cars.

From a spatial-zoning perspective, understanding and improving the spatio-temporal forecasting of short-term demand and supply-demand gap is immensely important to ride-hailing companies for determining the spatial allocation of fleet vehicles and reducing the spatial disequilibrium of supply-demand. However, due to the limited availability of ride-hailing data, less focus has been given to improve the spatio-temporal forecasting of demand and supply-demand gap in a ride-hailing system. Nevertheless, due to the similarity between taxi service and ride-hailing service, the concepts of supply-demand in the taxi system can shed important light on the ride-hailing system. Supply-demand equilibrium can be achieved theoretically if three parameters become equal: the rate of passengers demanding rides, the rate of available taxis, and the matching rate [3]. However, equilibrium cannot be maintained continuously due to information asymmetry [4]. Therefore, disequilibrium can occur from excessive supply or excessive demand, which is

unfavourable for both taxi companies and ride-hailing companies, thus necessitating them to stress on the accurate forecasting of demand and supply-demand gap. On the one hand, forecasting the demand can assist the ride-hailing companies in finding hotspot demand zones and determining appropriate fleet size. While on the other hand, forecasting the supply-demand gap serves as an indicator of the supply deficit of ride-hailing cars in each zone, which can be informative for implementing dynamic pricing strategies and incentivizing drivers as a means to deal with the disequilibrium issues. Nevertheless, there exist challenges in both the forecasting tasks due to spatio-temporal dependencies [5, 6], albeit not arising from the same factors. The relative difficulties in forecasting demand and supply-demand gap of a ride-hailing system can be addressed by two contrasting factors:

1) Local vs. non-local spatial dependencies: Ride-hailing supply-demand gap shows strong local spatial dependencies because of the continuous and rapid movement of vacant cars across nearby zones, while the passengers' zone of trip origin remains almost unchanged [7]. Therefore, the supply-demand gap of a zone can be fulfilled by the vacant cars of the surrounding zones, suggesting spatially correlated supply-demand gap patterns among the neighbouring zones. This claim is further justified by the highly fluctuating supply-demand gap of Didi for different zones of Beijing and Hangzhou, as shown in **Fig. 1**. However, for ride-hailing demand, non-local spatial dependencies (e.g., functional similarity, transportation connectivity) are considered in addition to the local spatial dependencies [8], all of which cannot be specified without relying on data mining.

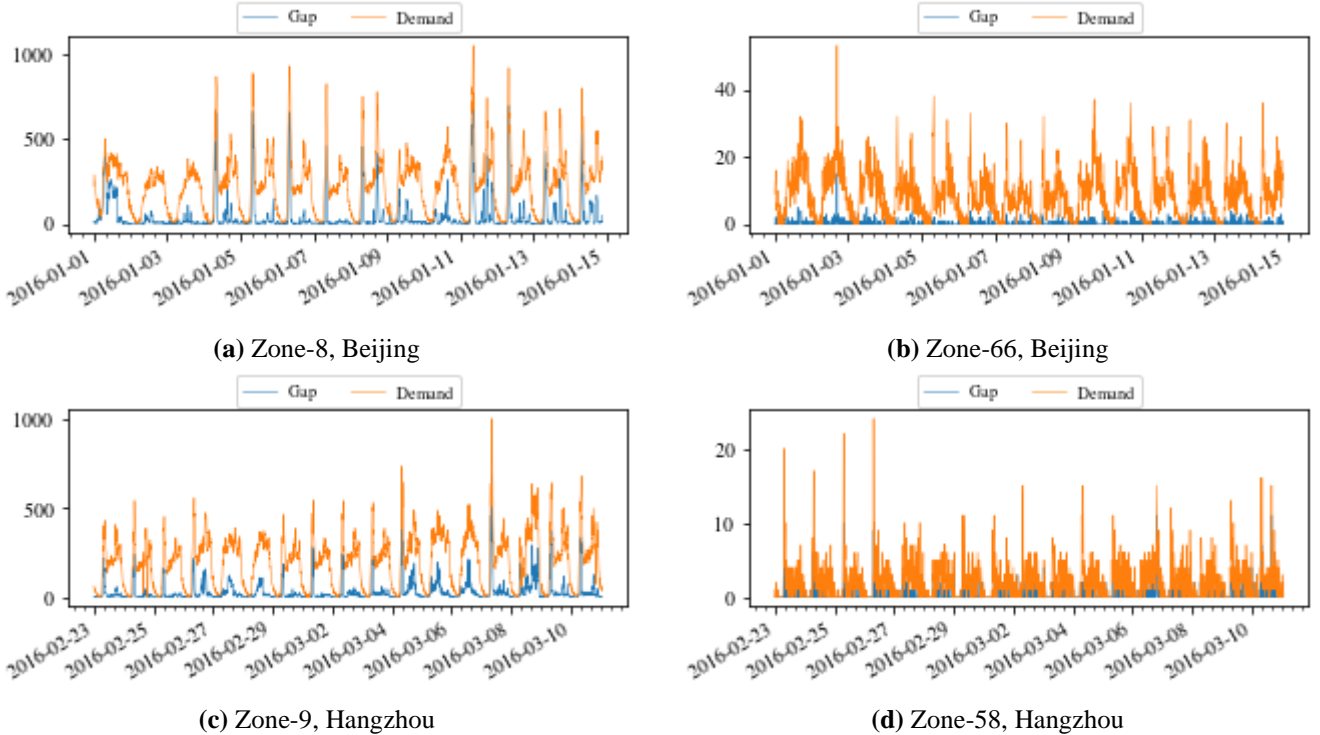


Fig. 1. Demand and supply-demand gap of various zones in Beijing and Hangzhou

2) Strong vs. weak temporal dependencies: Ride-hailing demand is found to have strong temporal dependencies due to almost recurring travel patterns of passengers every day, whereas ride-hailing supply-demand gap has weak temporal dependencies because of irregular fluctuations in the supply of vacant ride-hailing cars [7]. This phenomenon can be visualized from the demand and supply-demand gap trends of Didi in the two higher demand (supply-demand gap) zones of Beijing and Hangzhou, as shown in **Fig. 1(a)** and **Fig. 1(c)** respectively. However, both demand and supply-demand gap may have weak temporal dependencies in the relatively lower demand zones, as evident from the lower demand zones shown in **Fig. 1(b)** and **Fig. 1(d)**.

The most popular methods to detect spatio-temporal dependencies are the convolutional neural network (CNN) [9] and the recurrent neural network (RNN) [10], which are deep learning techniques with outstanding success in tasks related to computer vision and natural language processing. Earlier studies that applied deep learning for spatio-temporal forecasting generally divide the whole study area into several zones, and the historical features corresponding to the zones are utilized as inputs in the CNN or RNN. However, these methods require further considerations for spatio-temporal forecasting with ride-hailing data containing anonymized spatial adjacency information of the zones. Firstly, previous studies on spatio-temporal forecasting with deep learning require known spatial adjacency information for processing through two-dimensional CNN, which hinders the use of two-dimensional CNN in the case of data with anonymized spatial adjacency information. However, it is possible to process input features of such data as one-dimensional signals through one-dimensional CNN, based on recent findings that showed the applicability of CNN to learn from scrambled images [11]. Secondly, although gradient vanishing/exploding problem in the RNN for

capturing long-term temporal dependencies can be controlled by utilizing the independently recurrent neural network (IndRNN) [12], applying such method directly to learn temporal dependencies from spatio-temporal features is not possible due to the internal structure of the RNN.

In this paper, we put forward a spatio-temporal deep learning architecture, the feature importance integrated one-dimensional convolution and independently recurrent network (FOCIR-Net), to deal with the spatio-temporal dependencies for forecasting demand and supply-demand gap in a ride-hailing system with anonymized spatial adjacency information. The feature importance layer utilized in the architecture, in addition to providing an interpretation of the model, emphasizes more on strong predictors and attenuates weak predictors for each zone. To the best of the authors' knowledge, this paper, for the first time, integrates feature importance with a spatio-temporal deep learning architecture and applies one-dimensional CNN and zone-distributed IndRNN to deal with spatio-temporal dependencies in ride-hailing data with anonymized spatial adjacency information, which can be utilized to forecast both demand and supply-demand gap in a ride-hailing system. The major contributions of this study are as follows:

- 1) The FOCIR-Net detects spatial dependencies from the anonymized zones in a multivariate manner through one-dimensional CNN and temporal dependencies in an independent manner through zone-distributed IndRNN.
- 2) We integrate feature importance layer with a spatio-temporal deep learning architecture, which determines spatial weighting that adapts the model to accurately forecast both demand and supply-demand gap and also indicates the contribution of the corresponding input features for spatio-temporal forecasting.
- 3) We evaluate our proposed deep learning architecture with two real-world ride-hailing datasets of Didi from Beijing and Hangzhou. The comparison of the model

performance against extensively tuned statistical and machine learning models demonstrated the superiority of our model.

The remaining parts of the paper are arranged as follows. Section 2 reviews the previous studies on demand and supply-demand gap in a ride-hailing system. Section 3 defines the ride-hailing demand and supply-demand gap forecasting problem along with the associated variables. Section 4 describes the methodology and mathematical explanation of the proposed FOCIR-Net. Section 5 evaluates the proposed architecture with real-world datasets of Didi and compares the result with the benchmark models. The conclusions of the paper and future recommendations are provided in Section 6.

2. Related Works

Due to recent release of some ride-hailing and taxi datasets, a large amount of studies on spatio-temporal taxi/ride-hailing demand forecasting has been conducted in the last few years. Time series forecasting techniques have been utilized in some of the earlier studies. [13] designed a modified autoregressive integrated moving average (ARIMA) in an attempt to capture temporal periodicities with the short-term regular temporal patterns from the univariate time series data of historical taxi demand. The mathematical decomposition of their model further demonstrated that randomness in demand is due to contextual factors (e.g., weather condition, weekday/weekend). [4] developed an ensemble of ARIMA and time-varying Poisson models to explicitly deal with short-, medium-, and long-term temporal patterns in the historical taxi demand data. However, exogenous dependencies were not considered in these studies. To that end, linear regression combined with regularization was applied to features extracted through extensive feature engineering from taxi trip records and external datasets (e.g., point of interest (POI), weather condition, events information, traffic congestion) [14, 15]. These studies showed that forecasting error reduces with the inclusion of relevant additional factors. However, all of these abovementioned studies applied the same model to all spatial units without considering the spatial dependencies, which leads to unreliable demand forecast in some spatial units due to predictability heterogeneity [16].

In recent years, machine learning has been used widely by the researchers for ride-hailing demand forecasting problems because of its ability to learn complex features by processing massive datasets. [17] extracted important features with the least absolute shrinkage and selection operator (LASSO) that were utilized in random forest and support vector machines (SVM) for forecasting the short-term ride-hailing demand. However, these machine learning techniques do not explicitly model the spatio-temporal dependencies. To improve this limitation, hybrid modelling approaches have become useful. [18] processed spatially related features through an artificial neural network (ANN) and combined them with temporal features based on demand fluctuations for forecasting the ride-hailing demand through gradient boosting decision tree (GBDT). Their study successfully incorporated the spatial correlations in demand based on the similarity of neighbouring zones, however, ignoring temporal

dependencies in demand. [19] decomposed the ride-hailing demand time series into various frequency series through wavelet analysis, a signal processing technique, and trained SVM on the decomposed signals for forecasting the future ride-hailing demand by recomposing the predicted signals. Although their model successfully captured the non-stationarity in the time series of a zone, they disregarded the spatial dependencies among the zones. To consider spatial and temporal dependencies simultaneously, [20] combined boosting methods with the Gaussian conditional random field (GCRF) model, which can be used to predict ride-hailing demand by predicting demand distributions. However, spatio-temporal dependencies were modelled only based on historical demand, which limits the detection of various patterns in spatio-temporal dependencies.

Deep learning, a branch of machine learning, offers more flexibility to design sophisticated architectures for capturing spatial and temporal dependencies in the taxi/ride-hailing demand prediction. Some of the earlier studies [21, 22] applied variants of RNN, especially long short-term memory (LSTM) network [23], for capturing the temporal dependencies in taxi/ride-hailing demand forecasting. Recent studies [24, 25] processed the historical taxi/ride-hailing demand of different zones in a city as a sequence of images and the value of historical demand for a zone in a specific time interval was considered as a pixel value. By learning spatial features and correlations among the images through CNN, the model predicts the future taxi/ride-hailing demand. However, none of these studies was able to capture both spatial and temporal dependencies simultaneously, since CNN is unable to consider temporal patterns and RNN is unable to consider spatial patterns. To consider both spatial and temporal dependencies in a unified framework, [26] developed convolutional LSTM for precipitation forecasting by combining CNN and LSTM in an architecture that modified the LSTM cell by applying convolutions in the tensor-based LSTM cell. Extending from their work, some recent studies developed ensemble of convolutional LSTMs [3] and attention-based convolutional LSTM [27] for taxi/ride-hailing demand prediction task. [28] predicted ride-hailing demand forecasting by combining ride-hailing demand similarity-based graphs with local CNN and LSTM. [8] encoded the region-wise correlations based on predefined factors into multiple graphs, utilized them as input patterns for ride-hailing demand forecasting by learning spatial patterns through graph convolutions and temporal patterns through context gated recurrent neural network. These studies modelled spatio-temporal dependencies by processing input features either as pixels or graphs, however, these techniques cannot be applied directly to data with anonymized spatial adjacency information of the zones.

Although many studies have focused on taxi/ride-hailing demand forecasting problem, very few studies have explored the ride-hailing supply-demand gap forecasting problem. Some of the previous studies [29, 30] utilized ensemble of various machine learning algorithms for forecasting the region-wise supply-demand gaps. [30] applied a multi-layer ensemble of various machine learning algorithms (e.g., support vector machine, single XGBoost, bagging XGBoost, random forest, extra trees, and AdaBoost). The ensembles of various types of models were used to ensure diversity and stability in prediction, which

helped to reduce noise and overfitting. [29] applied a double ensemble technique to combine different GBDT models for forecasting supply-demand gaps in data-sparse situations. However, none of these studies explicitly modelled spatial and temporal dependencies for supply-demand gap forecasting task.

Deep learning techniques were applied in a few recent studies for supply-demand gap forecasting [6, 7]. Based on a deep residual network [31], [6] developed a deep learning architecture for forecasting the supply-demand gap of ride-hailing services. Their framework is extendible to include new features and requires less amount of feature engineering. Besides, they used embedding technique for capturing the similarity in the supply-demand gap patterns. [7] took advantage of improved partitioning by developing different types of hexagon-based convolutional neural networks (H-CNN) for different types of mapping functions (square, parity, and cube), and utilized a hexagon-based ensemble technique for forecasting supply-demand gaps. These studies addressed only either spatial or temporal dependencies, thus leaving room for further improvement in the forecasting of ride-hailing supply-demand gap.

Our work is different from the abovementioned studies in the following two aspects. Firstly, previous studies designed their models to deal with spatial and temporal dependencies for forecasting taxi/ride-hailing demand and ride-hailing supply-demand gap in a usual scenario, while our proposed deep learning architecture deals with spatio-temporal dependencies in ride-hailing data with anonymized spatial adjacency information. Secondly, the proposed architecture in this study addresses the problem of interpretability in the spatio-temporal deep learning models for spatio-temporal forecasting by utilizing spatial weighting through the feature importance layer, which was not done previously.

3. Preliminaries

Both ride-hailing demand and supply-demand gap are time-series forecasting tasks, where historical values of related variables can be important indicators for predicting future values. The historical values of the ride-hailing orders, the supplied quantity of ride-hailing cars, and the number of congested roads contain useful information regarding the spatio-temporal dependencies of demand and supply-demand gap. Additionally, weather condition, POI, time of day, and day of week also affects the demand and supply-demand gap of a region.

This section presents explanations of the variables and notations used in this paper along with the forecasting problem of demand and supply-demand gap.

Definition 1 (Space-time partitioning): For variable aggregation, the study area is divided into N non-overlapping uniformly sized zones $P = \{1, 2, 3, \dots, N\}$ and total days are divided into T time-slots $I = \{1, 2, 3, \dots, T\}$ of m minutes interval. The rest of the variables are defined based on the space-time partitioning.

Definition 2 (Spatio-temporal variables): The features that simultaneously vary in the spatial and temporal dimension are regarded as spatio-temporal variables. The types of the spatio-temporal variables utilized in this paper are as follows:

1) **Quantity supplied:** The quantity of ride-hailing cars supplied at all zones during the time-slot $t \in I$ is represented by the vector $S_t \in \mathbf{R}^N$, where $S_{t,p}$ is the total number of ride-hailing requests at zone $p \in P$ successfully matched with drivers by the ride-hailing platform, and $S_{t,p} \in [0, +\infty)$.

2) **Demand:** The total number of ride-hailing requests from a zone in a time interval is referred to as the demand, which includes both successfully matched and unanswered ride-hailing requests. The demand of all zones during the time-slot t is placed in the vector $D_t \in \mathbf{R}^N$. The demand at zone p during the time-slot t is denoted as $D_{t,p}$, where $D_{t,p} \geq S_{t,p}$.

3) **Supply-demand gap:** The total number of unmatched ride-hailing requests from a spatial zone in a time-slot is termed as the supply-demand gap. The supply-demand gap of all zones during the time-slot t is expressed as the vector $G_t \in \mathbf{R}^N$. The supply-demand gap of a zone p during the time-slot t is denoted by $G_{t,p}$, where $0 \leq G_{t,p} \leq D_{t,p}$.

4) **Traffic congestion:** The traffic congestion of all zones is denoted by the vector $TC_t \in \mathbf{R}^N$, where $TC_{t,p}$ represents the total number of congested roads belonging to a zone p during the time-slot t .

Definition 3 (Temporal variables): The temporal variables include the features that vary randomly across time, but not space. For maintaining consistency of input dimensions in our proposed architecture, these variables need to be repeated across the zones by utilizing the repeating function $f_{RZ}(\cdot; N) : \mathbf{R}^{1 \times M} \rightarrow \mathbf{R}^{N \times M}$, where M represents the number of feature categories. The following categories of temporal variables are included in this paper:

1) **Weather condition:** For the time-slot t , the weather conditions are represented by the row vector $wc_t \in \mathbf{R}^{1 \times C}$ consisting of C weather categories (e.g., sunny, rainy, snowy, etc.), where each category is encoded by one-hot encoding, i.e., $wc_{c,t} \in \{0, 1\}$. The weather condition vector wc_t is repeated across every zone to produce the weather condition matrix for the time-slot t , denoted by $WC_t \in \mathbf{R}^{N \times C}$.

2) **Temperature:** The temperature (in $^{\circ}\text{C}$) for the time-slot t is repeated across the zones to produce the temperature vector $WT_t \in \mathbf{R}^N$.

3) **Particulate matter:** For the time-slot t , the atmospheric particulate matter, $\text{PM}_{2.5}$ is repeated across the zones to form the particulate matter vector $WP_t \in \mathbf{R}^N$.

Definition 4 (Context variables): The context variables are either periodic or fixed across time. For spatio-temporal forecasting, these variables are either repeated across the zones by applying the repeating function f_{RZ} or repeated across the time-slots by utilizing the repeating function $f_{RT}(\cdot; T) : \mathbf{R}^N \rightarrow \mathbf{R}^{N \times 1 \times T}$. These are as follows:

1) **Temporal context:** Following [3], exploratory data analysis of the trends in demand and supply-demand gap

revealed two types of periodic contexts: time-of-day and day-of-peak. A time-slot t of a day belongs to one of the three 8-hour time-of-day intervals: sleep (first 8-hour), peak (mid-8-hour), and off-peak (last 8-hour), denoted by the row vector $\mathbf{cd}_t \in \mathbf{R}^{1 \times 3}$, where each interval i is one-hot encoded, i.e., $cd_{i,t} \in \{0,1\}$. Furthermore, a time-slot t falls into one of the day-of-week categories: weekday or weekend, represented by the vector $\mathbf{cw}_t \in \mathbf{R}$, where $cw_t \in \{0,1\}$. The temporal context vectors \mathbf{cd}_t and \mathbf{cw}_t are repeated across the zones to form the time-of-day matrix $\mathbf{CD}_t \in \mathbf{R}^{N \times 3}$ and the day-of-week vector $\mathbf{CD}_t \in \mathbf{R}^N$ respectively.

2) Spatial context: The spatial context refers to the number of POIs across the zones, denoted by the vector $\mathbf{cp}_p \in \mathbf{R}^N$, which is fixed across time. Therefore, it is repeated across the time-slots with the repeating function f_{RT} to form the spatial context vector for the time-slot t , represented by the vector $\mathbf{CP}_t \in \mathbf{R}^N$.

With the abovementioned definition of the variables, our spatio-temporal forecasting problem can be formulated as follows:

Problem: Given, the historical data of spatio-temporal variables and temporal variables up to b th previous time-slot starting from $t-1$, and known data of context variables at the time-slot t , we are required to predict the ground truth vector \mathbf{A}_t at the time-slot t for spatio-temporal forecasting of demand and supply-demand in ride-hailing system with anonymized spatial adjacency information.

4. Methodology

This section provides a brief description of the main components (i.e., feature importance layer, one-dimensional CNN, and zone-distributed IndRNN) as well as the proposed architecture.

4.1. Feature Importance Layer

Deep learning methods involve capturing complex interaction among features through multiple intermediate layers between inputs and outputs, which makes it difficult to interpret the contribution of the input features towards prediction. To address this issue, a number of methods [32–34] based on a one-to-one linear layer, usually utilized after the input layer, were implemented in deep artificial neural networks. The main idea of a one-to-one linear layer is similar to a fully connected layer except that a neuron in a one-to-one linear layer is connected with only one input rather than all inputs. This paper utilizes similar idea of feature importance layer except that the internal structure is modified for spatio-temporal forecasting, as expressed by the following function in Eq. (1):

$$f_{FeatureImportance}(\mathbf{X}_t) = \mathbf{X}_t \circ \sigma(\mathbf{W}^{(FI)}) \quad (1)$$

The operator \circ in Eq. (1) indicates Hadamard product, i.e., elementwise multiplication, between the input matrix $\mathbf{X}_t \in \mathbf{R}^{N \times F}$ for the time-slot t , containing N zones and F input features, and the outputs of the activation

function σ (e.g., linear, sigmoid, rectified linear unit (ReLU), hyperbolic tangent, etc.) for the weight matrix $\mathbf{W}^{(FI)} \in \mathbf{R}^{N \times F}$. For providing a fair advantage to all the features, i.e., all features are considered as equally important, training of the feature importance layer is initialized with uniform weights $\mathbf{W}^{(FI)} \sim U(-\gamma, +\gamma)$, where γ will depend on the type of activation function utilized in Eq. (1).

The theoretical justification of the feature importance layer utilized in this paper is similar to [32]. The weight matrix is updated during the training process, assigning larger weights to more important features and smaller weights to less important features. To ensure that the feature importance layer correctly captures the contribution of the input features, the weights and biases of the subsequent layers must not become zero during the training process. This is maintained by utilizing the L2-norm of regularization for the weights and biases used after the feature importance layer in the training algorithm. Furthermore, to ensure sparsity of $\mathbf{W}^{(FI)}$, the L1-norm of regularization for $\mathbf{W}^{(FI)}$ is included during the training of the architecture.

4.2. One-dimensional CNN

The CNN is a specialized neural network for detecting spatial dependencies by various types of filters (i.e., weights and bias) sliding over and convolving with the input. To address the spatial dependencies from anonymized zones in spatiotemporal forecasting, a one-dimensional CNN is utilized in this paper, where the filters are slid over only across the spatial dimension (i.e., anonymized zones) of the input with spatio-temporal feature columns. To detect same kind of spatial features with a filter, parameters of a filter are shared across the zones. The output feature vector of a filter k in a one-dimensional CNN layer can be expressed as follows:

$$\mathbf{Z}^{(k)} = \sigma(\mathbf{X}_t * \mathbf{W}^{(k)} + \mathbf{b}^{(k)}) \quad (2)$$

where $*$ is the convolution operator, \mathbf{X}_t is the input matrix convolved with the filter k , $\mathbf{Z}^{(k)} \in \mathbf{R}^N$ refers to the output feature vector for the filter, $\mathbf{W}^{(k)} \in \mathbf{R}^{E \times F}$ serves as the shared weight matrix of the filter with length E , and $\mathbf{b}^{(k)} \in \mathbf{R}^N$ is the shared bias vector of the filter. Therefore, the one-dimensional CNN layer with K filters applied to the input matrix \mathbf{X}_t can be represented by the function $f_{Conv1D} : \mathbf{R}^{N \times F} \rightarrow \mathbf{R}^{N \times K}$.

As an example, the inputs and outputs of a one-dimensional CNN with two convolutional layers are shown in **Fig. 2**. The first convolutional layer is comprised of two filters and the second convolutional layer is comprised of a single filter. The outputs of the convolutional layers are the columns of features, which are spatial patterns from the different types of input features utilized during one-dimensional convolutions with the filters. To keep the dimensions of inputs and outputs equal, zero paddings are used in the inputs of each convolutional layer. Although conventional CNN includes pooling layers, in order to prevent loss of spatial information, our one-dimensional CNN avoided the pooling layer following [24, 35].

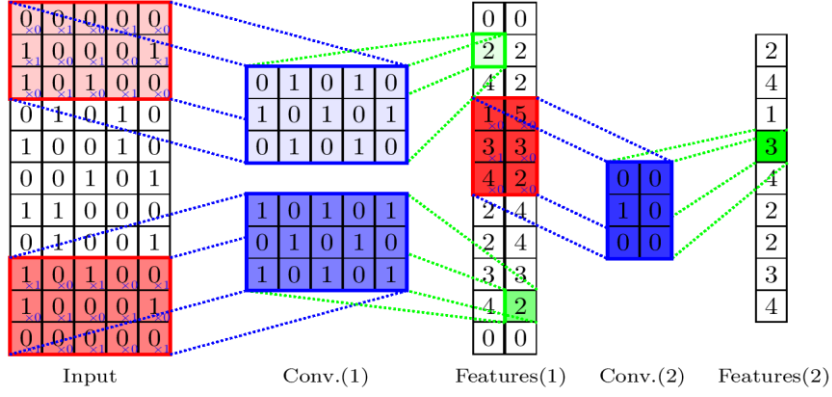


Fig. 2. One-dimensional CNN

4.3. Zone-distributed IndRNN

The RNN is an exclusive architecture for detecting temporal dependencies from time-series data where the features of one time-slot are correlated with the features of the previous time-slots. In comparison to the non-recurrent connections in conventional neural networks, the RNN has recurrent connections, i.e., the outputs of the hidden layer neurons from the previous time step of a sequence are utilized with the inputs of the current time step, which can be expressed by Eq. (3):

$$\mathbf{h}_t = \sigma(\mathbf{Ux}_t + \mathbf{Wh}_{t-1} + \mathbf{b}) \quad (3)$$

where $\mathbf{x}_t \in \mathbf{R}^F$ is the input vector at the current time step containing F features, $\mathbf{h}_t \in \mathbf{R}^H$ and $\mathbf{h}_{t-1} \in \mathbf{R}^H$ refer to the output vectors of size H representing hidden layer neurons of current and previous time step respectively, $\mathbf{U} \in \mathbf{R}^{H \times F}$ and $\mathbf{W} \in \mathbf{R}^{H \times H}$ serve as the weights for the input of the current step and the outputs of the previous step respectively, and $\mathbf{b} \in \mathbf{R}^H$ is the bias vector.

However, repeated multiplication of the recurrent hidden layer weight matrix during training results in the vanishing/exploding gradient problem in RNN that limits the storing of long-term information, which was tackled through LSTM by including additive updates in the hidden layer [23]. Despite the modification, training of LSTM can also suffer from vanishing gradient problem due to the application of non-linear activation functions [12], and can also face exploding gradient problem due to self-multiplication of the weight matrix [36]. To overcome these problems, IndRNN was proposed by replacing the entangled

recurrent connections in Eq. (3) with an elementwise multiplication, which can be utilized to learn temporal dependencies in spatio-temporal forecasting from the independent recurrent connections, as shown in Eq. (4):

$$\mathbf{h}_t = \sigma(\mathbf{Ux}_t + \mathbf{W}^{(I)} \circ \mathbf{h}_{t-1} + \mathbf{b}) \quad (4)$$

where $\mathbf{W}^{(I)} \in \mathbf{R}^H$ refers to the weight vector for the independently recurrent outputs of the last time step, which is regulated depending upon the activation function following the theoretical constraints provided by [12] for preventing vanishing/exploding gradient problem during training of the IndRNN.

An example of an unfolded IndRNN is shown in **Fig. 3**, which has two hidden layers (each containing H neurons where h represents an individual neuron) processing an input sequence containing three time steps. In the first hidden layer, neurons independently receive the input and the corresponding outputs of the previous time step, which facilitates the detection of various temporal dependencies from the input. The subsequent hidden layer further explores the correlation among the independently learned temporal dependencies. The output vector of the current time step t is the required prediction.

For detecting temporal dependencies in spatio-temporal forecasting, instead of a vector, the input of IndRNN at a time step is a matrix including the spatial dimension (i.e., zones), which requires the same IndRNN to be distributed across the zones independently with shared parameters. Therefore, we applied the IndRNN layer to the N zones of the input matrix \mathbf{X}_t by utilizing the function

$$f_{\text{ZoneDistributed(IndRNN)}} : f_{\text{IndRNN}}(\mathbf{x}_t) \rightarrow f_{\text{IndRNN}}(\mathbf{X}_t).$$

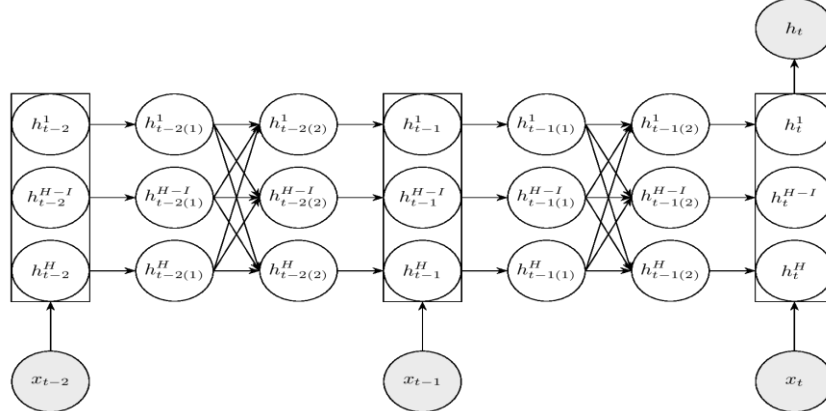


Fig. 3. IndRNN

4.4. Architecture of FOCIR-Net

The workflow of the FOCIR-Net architecture is shown in **Fig. 4**. All the inputs are initially spatially weighted through the feature importance layer to learn their contribution to the prediction. The weighted spatio-temporal variables are then passed through the layers of one-dimensional CNN to learn spatial dependencies, meanwhile, the weighted temporal variables together with the weighted spatiotemporal variables are passed through the stacked layers of zone-distributed IndRNN to learn temporal dependencies. Finally, the outputs of the one-dimensional CNN and zone-distributed IndRNN are then combined with the weighted context features to make the final prediction \mathbf{O}_t . According to the problem mentioned in section 3, the prediction target is the demand \mathbf{D}_t , or the supply-demand gap \mathbf{G}_t , which is denoted as ground truth \mathbf{A}_t . Techniques such as concatenating and reshaping are utilized in the architecture to adapt the input with architecture. To concatenate different vectors/matrix, the concatenation function $f_{Concatenate}$ is applied (e.g., $f_{Concatenate}(\mathbf{P}; \mathbf{Q}) : \mathbf{R}^{N \times N} \rightarrow \mathbf{R}^{N \times 2}$, where $\mathbf{P} \in \mathbf{R}^N$ and $\mathbf{Q} \in \mathbf{R}^N$ are the vectors to be concatenated). To meet the requirement of time steps for the zone-distributed IndRNN, corresponding inputs are reshaped through the reshaping function $f_{Reshape}(\mathbf{J}; Y) : \mathbf{R}^{N \times B} \rightarrow \mathbf{R}^{N \times Y \times (B/Y)}$, where \mathbf{J} is the matrix with B features to be reshaped to Y time-steps.

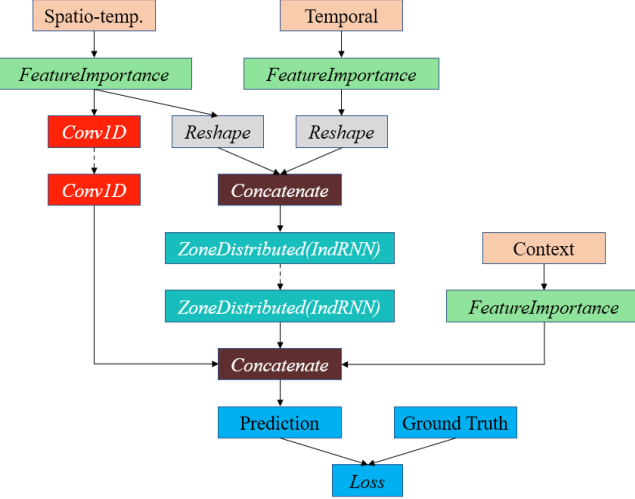


Fig. 4. Workflow of FOCIR-Net architecture

The training of the FOCIR-Net involves minimizing the mean squared error between the predicted values and the ground truth, which is achieved through the loss function f_{Loss} . The objective of the loss function applied in our architecture including regularization terms can be expressed as Eq. (5):

$$\min_{\mathbf{W}^{(A)}, \mathbf{W}^{(FI)}, b} f_{Loss} = \|\mathbf{O}_t - \mathbf{A}_t\|_2^2 + \alpha \|\mathbf{W}^{(A)}\|_2^2 + \beta \|\mathbf{W}^{(FI)}\|_1 \quad (5)$$

where $\mathbf{A}_t \in \mathbf{R}^N$ is the ground truth vector, $\mathbf{W}^{(A)}$ refers to all parameters of the FOCIR-Net except the feature importance layer parameter $\mathbf{W}^{(FI)}$, and α , β are the regularization parameters. The L1- and L2-norm of regularization are utilized in accordance with the requirements of the feature importance layer, which also assists in avoiding overfitting issues.

5. Experiments and Discussions

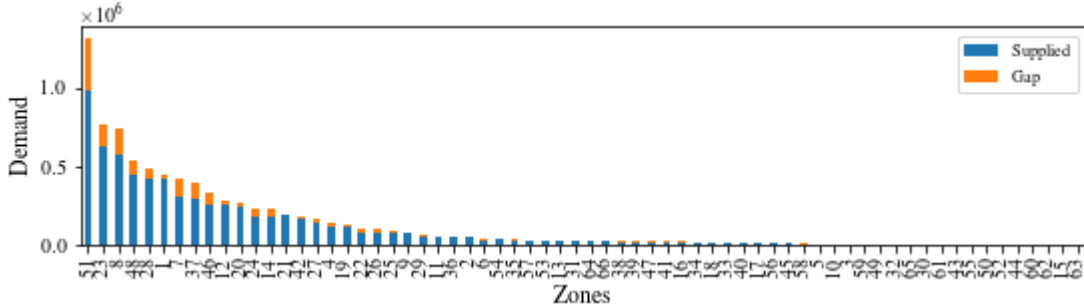
This section presents the experiments on real-world data and the discussion of their results. Furthermore, model ablation of the proposed FOCIR-Net is also provided. Finally, the interpretations of the FOCIR-Net models are provided at the end of the section.

5.1. Data description and preprocessing

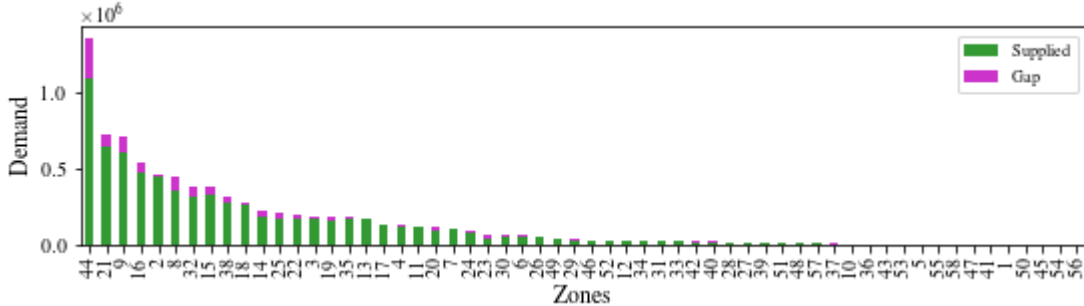
Publicly released ride-hailing datasets [37] from two cities of China, Beijing and Hangzhou, are selected for the experiments in this paper. Didi divided each city into several square zones by applying geohashing and identified each zone with a unique ID, anonymizing the adjacency information among the zones.

We utilized the Beijing dataset spanning from 1st January 2016 to 20th January 2016 and the Hangzhou dataset spanning from 23rd February 2016 to 17th March 2016. To construct time-series data for each zone, the total timespan is divided into equal interval time-slots. Considering the small length of the datasets and focusing on short-term forecasting, each day in the datasets is therefore divided into 144 time-slots of 10 minutes interval. Furthermore, the total time-slots in a zone are split into training, validation, and testing sets for our experiments. Around 30% of the time-slots are reserved for validation and testing, and the rest of the data are used in training the models.

Both the datasets contain information around 8.5 million ride-hailing orders. The order information provides anonymized information of each order including driver ID, passenger ID, and, trip origin and destination geohashes. Besides, date and time of the orders are also available in the datasets. The unfulfilled orders are marked by a ‘null’ driver ID, which is useful information for calculating the supply-demand gaps in a zone for a time-slot. Furthermore, in order to find the demand and quantity supplied of each zone from the order information, the orders including ‘null’ driver IDs and orders excluding ‘null’ driver IDs are aggregated, respectively, for a timeslot. For both the datasets, around 50 percent of the time-slots are found to have zero supply-demand gaps, around 17 percent of which are due to zero demand, indicating that orders in around 33 percent time-slots are fully matched by the platform. The zone-wise distribution of total demand, including the proportions of quantity supplied and supply-demand gap, is shown in **Fig. 5(a)** and **Fig. 5(b)** for Beijing and Hangzhou respectively. In general, relatively higher demand zones tend to show a higher supply-demand gap in both datasets.



(a) Average demand distribution in Beijing



(b) Average demand distribution in Hangzhou

Fig. 5. Average demand distribution across zones

In addition to the order information, zone-wise traffic congestion information for each time-slot is included, indicating the number of roads at different congestion levels that is aggregated to get an idea of the overall congestion of a zone for a time-slot. Furthermore, 10 minutes interval city-level weather information (i.e., weather category, PM 2.5, and temperature) and zone-wise time-invariant POI information are also provided in the datasets. The facilities in different POI classes are aggregated for our experiments.

5.2. Model Evaluations

The proposed FOCIR-Net is compared against a set of benchmark algorithms and an ablation analysis of FOCIR-Net is conducted. For a fair comparison, all models utilized the same lookback window up to sixth previous time-slot. The settings of FOCIR-Net are decided by tuning of the hyperparameters. The finalized settings of the hyperparameters are presented in **Table 1**.

In order to assess the performance of FOCIR-Net, a number of benchmark models are considered, which are extensively tuned by utilizing automated machine learning frameworks. They are as follows:

Table 1. Hyperparameter settings of FOCIR-Net

Hyperparameter settings	
(a) Feature Importance Layer	Weight initialization: uniform; activation: sigmoid
(b) 1D-CNN	Layers: 2 layers; filters: 200 in 1 st layer; 400 in 2 nd layer; filter length: 3-11 Weight initialization: uniform; activation: ReLU
(c) Zone-distributed IndRNN	Layers: 2 layers; hidden units: 4 units per layer Weight initialization: uniform; activation: tanh/ReLU
(d) Fully Connected Layer	Weight initialization: uniform; activation: ReLU
(e) Model Training	Optimizer: Adam [43]; learning rate: 0.001; batch size: 32 Regularization: L1 = 0.001, L2 = 0.001; early stopping: patience = 100 epochs

1) Gradient Boosting Machine (GBM): The GBM [38] is an ensemble method that is built upon several additive regression trees through the utilization of the gradient descent technique.

2) Extreme Gradient Boosting (XGBoost): The XGBoost [39], a modified version of GBM, is a popular algorithm that has topped in many machine learning competitions. The XGBoost algorithm utilizes regularized gradient boosting to control overfitting.

3) Random Forest (RF): The RF [40] is an ensemble method that utilizes several weak learner regression trees. The splitting of the trees is determined by finding the most appropriate discriminative threshold for a subset of features.

4) Extremely Randomized Trees (XRT): The XRT [41] is similar to the RF except that it extracts randomly generated thresholds for each feature and the best threshold is utilized for splitting the trees.

5) Generalized Linear Model (GLM): The GLM [42] is a generalization of the linear regression that allows any of the exponential family of distributions in the errors of the outcome variable. Since our outcome is continuous, our GLM implementation assumes Gaussian distribution.

6) Artificial Neural Network (ANN): The ANN [44] contains a feedforward neural network with several hidden layers to learn hierarchical representation from the input features. Our ANN is trained with a mini-batch size of 1.

7) Autoregressive Integrated Moving Average (ARIMA): The ARIMA [45] is a time series forecasting method that removes trends from the data and estimates relationship and error from the past observations to forecast future values. Our implementation of ARIMA includes explanatory variables with conventional ARIMA.

It is noteworthy to mention that, all the benchmarks excluding ARIMA utilized the same input features as FOCIR-Net, whereas ARIMA utilized all input features except the categorical ones.

In addition to the abovementioned models, model ablation of FOCIR-Net is also conducted by removing the model components one at a time. The following configurations are tested:

1) One-dimensional Convolution and Independently Recurrent Network (OCIR-Net): The OCIR-Net includes all model components except the feature importance layer. The input features are directly fed into the model without any spatial weighting.

2) Feature Importance Integrated One-dimensional Convolution Network (FOC-Net): The zone-distributed IndRNN is removed in this configuration. In this model, the weighted spatio-temporal features are processed through the one-dimensional CNN and the rest of the weighted features (i.e., temporal and context features) are concatenated with the outputs of the one-dimensional CNN to make the final prediction.

3) Feature Importance Integrated Independently Recurrent Network (FIR-Net): The FIR-Net excludes the one-dimensional CNN. Only temporal dependencies are considered in this model.

The performances of the models utilized in this paper are evaluated with three metrics: mean absolute error (MAE), root mean squared error (RMSE), and symmetric mean absolute percentage error (sMAPE), which can be computed by using Eq. (6)-(8):

Table 2. Performances evaluation of FOCIR-Net and benchmark models

Model	Metrics (Demand)				Metrics (Supply-demand gap)			
	MAE	RMSE	sMAPE	Time (s)	MAE	RMSE	sMAPE	Time (s)
(a) Beijing	FOCIR-Net	6.45	16.77	0.1867	229	3.34	14.56	0.2288
	XGBoost	6.88	19.07	0.2009	3.68	3.70	16.74	0.2952
	GBM	7.00	18.91	0.2186	3.99	3.77	16.53	0.3053
	XRT	7.04	19.43	0.1994	78.40	3.91	17.07	0.3045
	RF	7.23	22.18	0.2006	79.45	3.90	16.60	0.3044
	GLM	7.65	19.78	0.2537	0.44	4.61	16.80	0.3998
	ANN	14.48	25.57	0.4250	33.21	5.34	19.09	0.4671
	ARIMA	8.22	20.79	0.2152	262.73	4.57	17.52	0.3321
(b) Hangzhou	FOCIR-Net	6.82	16.34	0.1626	237	2.92	13.45	0.2257
	XGBoost	7.25	17.35	0.1770	17.18	3.06	13.46	0.2873
	GBM	7.12	17.09	0.1761	10.69	3.06	13.52	0.3018
	XRT	7.19	17.43	0.1734	106.97	3.12	13.64	0.2898
	RF	7.18	17.28	0.1730	103.09	3.14	13.80	0.2896
	GLM	7.70	18.05	0.2070	0.42	3.44	14.55	0.3222
	ANN	7.80	18.12	0.2137	7.67	3.41	14.07	0.3426
	ARIMA	11.33	26.32	0.2617	242.73	7.88	28.60	0.4627

$$MAE = \frac{1}{n} \sum_{i=1}^n |\mathbf{O}_i - \mathbf{A}_i| \quad (6)$$

$$RMSE = \sqrt{\frac{1}{n} \sum_{i=1}^n (\mathbf{O}_i - \mathbf{A}_i)^2} \quad (7)$$

$$sMAPE = \frac{1}{n} \sum_{i=1}^n \frac{|\mathbf{O}_i - \mathbf{A}_i|}{|\mathbf{O}_i| + |\mathbf{A}_i| + 1} \quad (8)$$

where \mathbf{O}_i and \mathbf{A}_i are the predicted vector and ground truth vector, respectively, at time-slot i in the test set with size n time-slots. Since our target value contains zero and sMAPE produces inaccurate statistics when encountered with zero, therefore, a modified sMAPE [4] is utilized.

Our proposed architecture is trained on a server with 4 Core (hyper-threaded) Xeon processor (2.30 GHz), 25 GB RAM, and a Tesla K-80 GPU. The FOCIR-Net is written in Python 3 using Keras [46] with Tensorflow [47] backend. All the benchmarks except ARIMA are implemented in H2O AutoML [48], while ARIMA is implemented in Pmdarima [49].

The performances of the FOCIR-Net and the benchmark models are reported in **Table 2**. It is evident that for all metrics, the FOCIR-Net outperforms all the benchmark models using both datasets. For demand forecasting, the FOCIR-Net has 11.32 % and 4.38 % lower RMSE than the best benchmark GBM for Beijing and Hangzhou, respectively. Furthermore, the FOCIR improves the MAE by 6.25 % and 4.21 % than the best benchmarks XGBoost for Beijing and GBM for Hangzhou, respectively. For supply-demand gap forecasting, 9.73 % and 11.92 % improvement in RMSE and MAE, respectively, are seen for the FOCIR-Net than the best benchmarks GBM and XGBoost in Beijing, while 4.58 % improvement in MAE and marginal improvement of RMSE is found for FOCIR-Net than the best benchmark XGBoost in Hangzhou. However, the FOCIR-Net has more than 6 % improvement of sMAPE than the best benchmark XGBoost for supply-demand gap forecasting in both datasets.

Table 3. Ablation analysis of FOCIR-Net

	Model	Metrics (Demand)				Metrics (Supply-demand gap)			
		MAE	RMSE	sMAPE	Time (s)	MAE	RMSE	sMAPE	Time (s)
(a) Beijing	OCIR-Net	6.71	17.19	0.1942	152	3.38	14.67	0.2351	691
	FOC-Net	6.49	16.96	0.1958	229	3.42	14.98	0.2372	260
	FIR-Net	19.61	51.00	0.3116	3150	7.44	33.13	0.3057	1982
(b) Hangzhou	OCIR-Net	7.02	16.68	0.1718	394	2.93	13.59	0.2234	326
	FOC-Net	7.04	16.66	0.1693	312	3.08	13.91	0.2298	236
	FIR-Net	7.71	18.25	0.1928	777	3.61	15.25	0.2583	726

Table 3 presents the performance evaluation of the models utilized in the ablation analysis of the FOCIR-Net. For both datasets, improvements around 1-2 % in the MAE and RMSE of the FOCIR-Net are observed with respect to the corresponding values of MAE and RMSE in OCIR-Net and FOC-Net, respectively, which indicates that the feature importance layer and zone-distributed IndRNN adds to the performance of the FOCIR-Net. Most importantly, the large drop in performance with a huge increase in training time in the FIR-Net indicates that the processing of the spatio-temporal variables through the one-dimensional CNN plays the most important role in the FOCIR-Net.

5.3. Model Interpretations

In this paper, the weights utilized by the feature importance layer in the FOCIR-Net are processed through a sigmoid function, which bounds the learned weights between 0 and 1. This is useful to interpret the contributions of the input features in the FOCIR-Net. In order to

separately explain the contribution of the features temporally and spatially, the outputs of the feature importance layer are averaged spatially and temporally, respectively. For conciseness, only the results for Hangzhou data is presented here.

Fig. 6(a) and **Fig. 6(b)** presents the feature importance rankings of the spatially averaged features for demand and supply-demand gap forecasting, respectively. It is intriguing to find that the historical values of the demand, quantity supplied and congestion have a major contribution to the prediction. The least contribution among the spatio-temporal features is seen for the historical values of the supply-demand gap, which is mainly because of irregular patterns in the historical supply-demand gap. It is also found that almost all the context features (except the sleep hour in the supply-demand gap forecasting) are found to have more contribution towards prediction while comparing with the temporal features. Among the temporal features, the temperature and the PM2.5 for the interval (t-5) and (t-6) have relatively higher importance than the other temporal features.

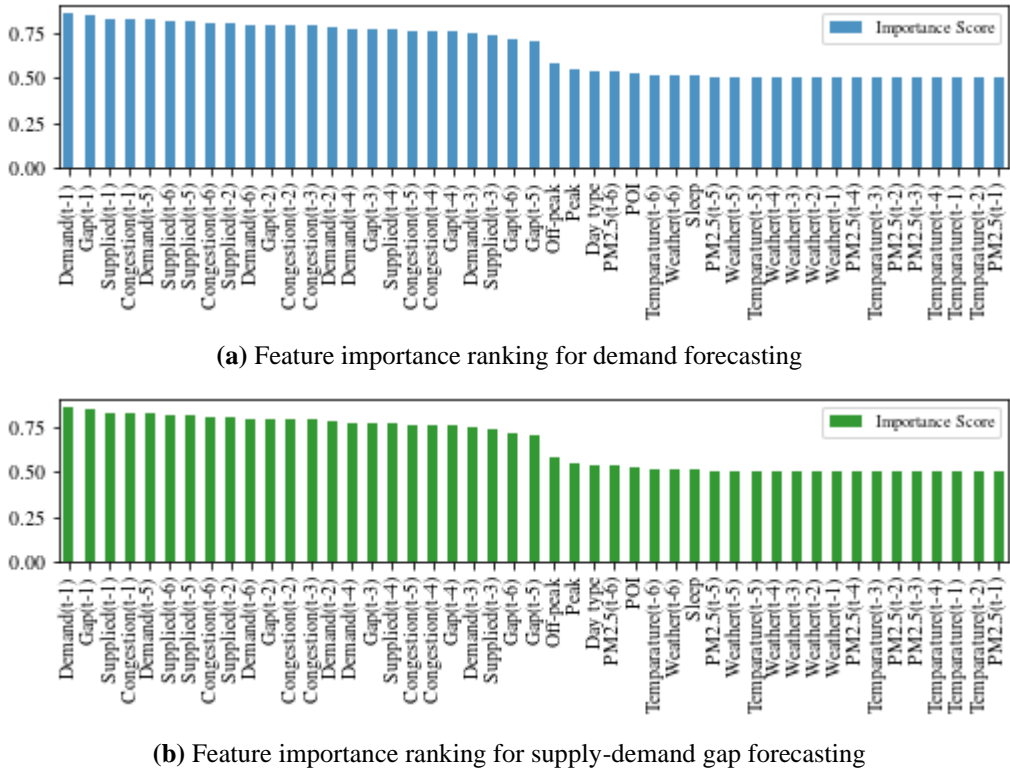


Fig. 6. Spatially averaged feature importance

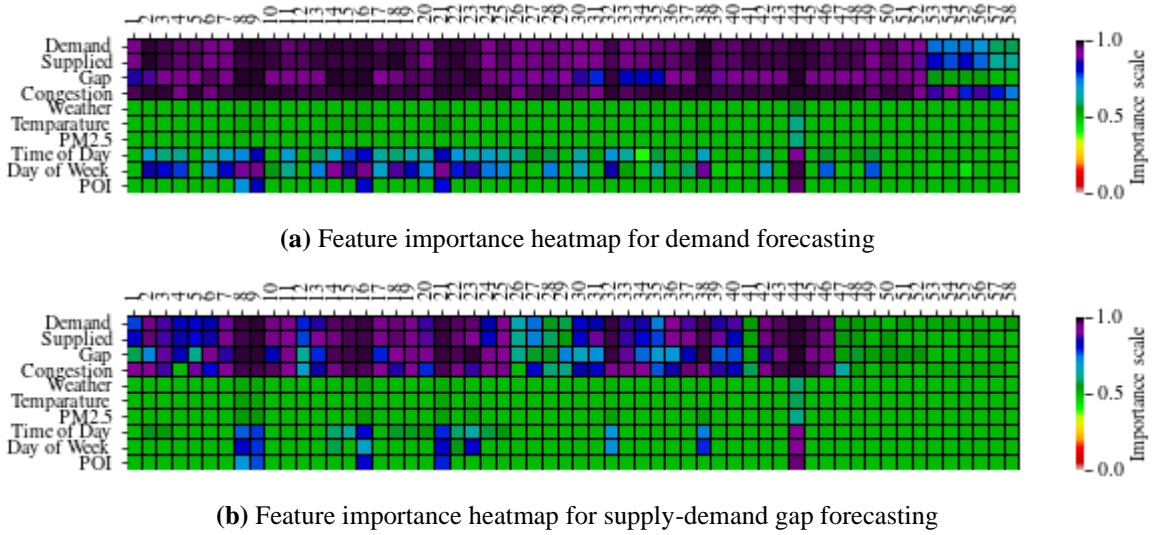


Fig. 7. Temporally averaged feature importance

The temporally averaged features are presented in the heatmaps in **Fig. 7(a)** and **Fig. 7(b)**. It is found that importance of the spatio-temporal features and the context features are not uniform across the zones, while importance of the temporal features are mostly uniform across the zones except for the zone-44, which has the highest total of demand and supply-demand gap. In general, it is found that the features of the higher demand (supply-demand gap) zones are more important to the FOCIR-Net for prediction than that of the lower demand (supply-demand gap) zones.

6. Conclusions

In this paper, a spatio-temporal deep learning architecture, FOCIR-Net, is proposed for forecasting both demand and supply-demand gap in a ride-hailing system with anonymized spatial adjacency information. The proposed architecture integrates feature importance layer with a spatio-temporal deep learning architecture composed of one-dimensional CNN and zone-distributed IndRNN. The architecture of FOCIR-Net processes different types of spatio-temporal, temporal and context features by spatially weighting them through the feature importance layer and learning spatial and temporal dependencies from the corresponding features through the one-dimensional CNN and zone-distributed IndRNN. The weights learned from the feature importance layer further assists in the ranking of the features and interpreting the model. The proposed FOCIR-Net is compared against several benchmark models including time-series models such as ARIMA, and machine learning algorithms such as XGBoost, GBM, RF, XRT, GLM, and ANN. The models are tested with two real-world datasets of Didi from Beijing and Hangzhou, which shows the superiority of FOCIR-Net in terms of MAE, RMSE, and sMAPE in both demand and supply-demand forecasting tasks. An ablation analysis of the FOCIR-Net is conducted, which shows that the processing of the spatio-temporal variables through the one-dimensional CNN is the most crucial part of the FOCIR-Net. Finally, interpretations of the models are provided based on the outputs of the feature importance layer.

The proposed architecture demonstrates the applicability of spatio-temporal deep learning for forecasting with anonymized spatial adjacency information.

Furthermore, model interpretation shows that the feature importance layer can assist the researchers to get a better understanding of the spatio-temporal deep learning models. Nevertheless, our paper is not above limitations. Detailed information for some of the features such as weather categories, traffic congestion levels, and POI are unavailable in the datasets due to confidentiality issues that limited us from utilizing more features. The proposed architecture will be tested against a large number of features in the future by extending our architecture for station-based platforms such as taxi and bike-sharing. Furthermore, model interpretations show generalizations of some of the features between the demand and supply-demand gap models, which indicate that developing a multi-task learning architecture for simultaneous forecasting of demand and supply-demand gap can be an interesting area for future research.

7. Acknowledgements

This research is funded by Miyan Research Institute, International University of Business Agriculture and Technology. The authors are thankful to Didi Chuxing for the publicly released datasets.

8. References

- 1 Chen, X. (Michael), Zahiri, M., Zhang, S.: ‘Understanding ridesplitting behavior of on-demand ride services: An ensemble learning approach’*Transp. Res. Part C Emerg. Technol.*, 2017, **76**, pp. 51–70.
- 2 Clewlow, R.R., Mishra, G.S.: ‘Disruptive Transportation: The Adoption, Utilization, and Impacts of Ride-Hailing in the United States’ (2017)
- 3 Ke, J., Zheng, H., Yang, H., Chen, X. (Michael): ‘Short-term forecasting of passenger demand under on-demand ride services: A spatio-temporal deep learning approach’*Transp. Res. Part C Emerg. Technol.*, 2017, **85**, (October), pp. 591–608.
- 4 Moreira-Matias, L., Gama, J., Ferreira, M., Mendes-Moreira, J., Damas, L.: ‘Predicting Taxi–Passenger Demand Using Streaming Data’*IEEE Trans. Intell. Transp. Syst.*, 2013, **14**, (3), pp. 1393–1402.
- 5 Chiang, M.-F., Hoang, T.-A., Lim, E.-P.: ‘Where are the passengers?: a grid-based gaussian mixture model for taxi bookings’, in ‘Proceedings of the 23rd SIGSPATIAL International Conference on Advances in Geographic Information Systems - GIS ’15’ (ACM Press, 2015), pp. 1–10
- 6 Wang, D., Cao, W., Li, J., Ye, J.: ‘DeepSD: Supply-demand prediction for online car-hailing services using deep neural networks’, in ‘Proceedings - International Conference on Data

Engineering' (2017), pp. 243–254

7 Ke, J., Yang, H., Zheng, H., *et al.*: 'Hexagon-Based Convolutional Neural Network for Supply-Demand Forecasting of Ride-Sourcing Services' *IEEE Trans. Intell. Transp. Syst.*, 2018, pp. 1–14.

8 Geng, X., Li, Y., Wang, L., *et al.*: 'Spatiotemporal Multi-Graph Convolution Network for Ride-Hailing Demand Forecasting', in 'Proceedings of the AAAI Conference on Artificial Intelligence' (2019), pp. 3656–3663

9 LeCun, Y., Haffner, P., Bottou, L., Bengio, Y.: 'Object recognition with gradient-based learning', in 'Lecture Notes in Computer Science (including subseries Lecture Notes in Artificial Intelligence and Lecture Notes in Bioinformatics)' (Springer, Berlin, Heidelberg, 1999), pp. 319–345

10 Williams, R.J., Zipser, D.: 'A Learning Algorithm for Continually Running Fully Recurrent Neural Networks' *Neural Comput.*, 1989, **1**, (2), pp. 270–280.

11 Brendel, W., Bethge, M.: 'Approximating CNNs with Bag-of-local-Features models works surprisingly well on ImageNet' *7th Int. Conf. Learn. Represent. ICLR 2019*, 2019.

12 Li, S., Li, W., Cook, C., Zhu, C., Gao, Y.: 'Independently Recurrent Neural Network (IndRNN): Building A Longer and Deeper RNN', in 'Proceedings of the IEEE Computer Society Conference on Computer Vision and Pattern Recognition' (2018), pp. 5457–5466

13 Li, X., Pan, G., Wu, Z., *et al.*: 'Prediction of urban human mobility using large-scale taxi traces and its applications' *Front. Comput. Sci. China*, 2012, **6**, (1), pp. 111–121.

14 Wu, F., Wang, H., Li, Z.: 'Interpreting traffic dynamics using ubiquitous urban data', in 'Proceedings of the 24th ACM SIGSPATIAL International Conference on Advances in Geographic Information Systems - GIS '16' (ACM Press, 2016), pp. 1–4

15 Tong, Y., Chen, Y., Zhou, Z., *et al.*: 'The Simpler The Better: A Unified Approach to Predicting Original Taxi Demands based on Large-Scale Online Platforms', in 'Proceedings of the 23rd ACM SIGKDD International Conference on Knowledge Discovery and Data Mining - KDD '17' (ACM Press, 2017), pp. 1653–1662

16 Zhao, K., Khryashchev, D., Freire, J., Silva, C., Vo, H.: 'Predicting taxi demand at high spatial resolution: Approaching the limit of predictability', in '2016 IEEE International Conference on Big Data (Big Data)' (IEEE, 2016), pp. 833–842

17 Liu, J., Cui, E., Hu, H., Chen, X., Chen, X.M., Chen, F.: 'Short-term forecasting of emerging on-demand ride services', in '2017 4th International Conference on Transportation Information and Safety, ICTIS 2017 - Proceedings' (2017), pp. 489–495

18 Wei, H., Wang, Y., Wo, T., Liu, Y., Xu, J.: 'ZEST: A Hybrid Model on Predicting Passenger Demand for Chauffeured Car Service', in 'Proceedings of the 25th ACM International Conference on Information and Knowledge Management - CIKM '16' (ACM Press, 2016), pp. 2203–2208

19 Li, Y., Lu, J., Zhang, L., Zhao, Y.: 'Taxi Booking Mobile App Order Demand Prediction Based on Short-Term Traffic Forecasting' *Transp. Res. Rec. J. Transp. Res. Board*, 2017, **2634**, (1), pp. 57–68.

20 Qian, X., Ukkusuri, S. V., Yang, C., Yan, F.: 'Forecasting short-term taxi demand using boosting-GCRF', in 'The 6th International Workshop on Urban Computing (UrbComp 2017)' (2017)

21 Wang, C., Hao, P., Wu, G., Qi, X., Barth, M.: 'Predicting the Number of Uber Pickups by Deep Learning', in 'Transportation Research Board 97th Annual Meeting' (2018)

22 Xu, J., Rahmatizadeh, R., Boloni, L., Turgut, D.: 'Real-Time Prediction of Taxi Demand Using Recurrent Neural Networks' *IEEE Trans. Intell. Transp. Syst.*, 2018, **19**, (8), pp. 2572–2581.

23 Hochreiter, S., Schmidhuber, J.: 'Long Short-Term Memory' *Neural Comput.*, 1997, **9**, (8), pp. 1735–1780.

24 Jiang, W., Zhang, L.: 'Geospatial Data to Images: A Deep-Learning Framework for Traffic Forecasting' *Tsinghua Sci. Technol.*, 2019, **24**, (1), pp. 52–64.

25 Wang, C., Hou, Y., Barth, M.: 'Data-Driven Multi-step Demand Prediction for Ride-Hailing Services Using Convolutional Neural Network', in 'Advances in Intelligent Systems and Computing' (2020), pp. 11–22

26 Shi, X., Chen, Z., Wang, H., Yeung, D.Y., Wong, W.K., Woo, W.C.: 'Convolutional LSTM network: A machine learning approach for precipitation nowcasting', in 'Advances in Neural Information Processing Systems' (2015), pp. 802–810

27 Zhou, X., Shen, Y., Zhu, Y., Huang, L.: 'Predicting Multi-step Citywide Passenger Demands Using Attention-based Neural Networks', in 'Proceedings of the Eleventh ACM International Conference on Web Search and Data Mining - WSDM '18' (ACM Press, 2018), pp. 736–744

28 Yao, H., Wu, F., Ke, J., *et al.*: 'Deep Multi-View Spatial-Temporal Network for Taxi Demand Prediction', in 'Thirty-Second AAAI Conference on Artificial Intelligence (AAAI-18)' (2018)

29 Zhang, X., Wang, X., Chen, W., Tao, J., Huang, W., Wang, T.: 'A Taxi Gap Prediction Method via Double Ensemble Gradient Boosting Decision Tree', in 'Proceedings - 3rd IEEE International Conference on Big Data Security on Cloud, BigDataSecurity 2017, 3rd IEEE International Conference on High Performance and Smart Computing, HPSC 2017 and 2nd IEEE International Conference on Intelligent Data and Security (IEEE, 2017), pp. 255–260

30 Wang, R.: 'Supply-demand Forecasting For a Ride-Hailing System'. University of California, Irvine, 2017

31 He, K., Zhang, X., Ren, S., Sun, J.: 'Deep Residual Learning for Image Recognition', in '2016 IEEE Conference on Computer Vision and Pattern Recognition (CVPR)' (IEEE, 2016), pp. 770–778

32 Borisov, V., Haug, J., Kasneci, G.: 'CancelOut: A Layer for Feature Selection in Deep Neural Networks', in 'Lecture Notes in Computer Science (including subseries Lecture Notes in Artificial Intelligence and Lecture Notes in Bioinformatics)' (Springer Verlag, 2019), pp. 72–83

33 Lu, Y.Y., Fan, Y., Lv, J., Noble, W.S.: 'Deeppink: Reproducible feature selection in deep neural networks', in 'Advances in Neural Information Processing Systems' (2018), pp. 8676–8686

34 Li, Y., Chen, C.Y., Wasserman, W.W.: 'Deep feature selection: Theory and application to identify enhancers and promoters' *J. Comput. Biol.*, 2016, **23**, (5), pp. 322–336.

35 Shen, B., Liang, X., Ouyang, Y., Liu, M., Zheng, W., Carley, K.M.: 'StepDeep: A Novel Spatial-temporal Mobility Event Prediction Framework based on Deep Neural Network Bilong', in 'Proceedings of the 24th ACM SIGKDD International Conference on Knowledge Discovery & Data Mining - KDD '18' (ACM Press, 2018), pp. 724–733

36 Sutskever, I., Vinyals, O., Le, Q. V.: 'Sequence to sequence learning with neural networks', in 'Advances in Neural Information Processing Systems' (2014), pp. 3104–3112

37 Didi: 'Didi Di-Tech Challenge Algorithm Competition', <http://web.archive.org/web/20170311212917/http://research.xiaojukeji.com/competition/main.action?competitionId=DiTech2016>

38 Friedman, J.H.: 'Greedy Function Approximation: A Gradient Boosting Machine' *Ann. Stat.*, 2001, **29**, (5), pp. 1189–1232.

39 Chen, T., Guestrin, C.: 'XGBoost: A scalable tree boosting system', in 'Proceedings of the ACM SIGKDD International Conference on Knowledge Discovery and Data Mining' (Association for Computing Machinery, 2016), pp. 785–794

40 Liaw, A., Wiener, M.: 'Classification and Regression by randomForest' *R News*, 2002, **2**, (3), pp. 18–22.

41 Geurts, P., Ernst, D., Wehenkel, L.: 'Extremely randomized trees' *Mach. Learn.*, 2006, **63**, (1), pp. 3–42.

42 Nelder, J.A., Wedderburn, R.W.M.: 'Generalized Linear Models' *J. R. Stat. Soc. Ser. A*, 1972, **135**, (3), pp. 370–384.

43 Kingma, D.P., Ba, J.L.: 'Adam: A method for stochastic optimization', in '3rd International Conference on Learning Representations, ICLR 2015 - Conference Track Proceedings' (2015)

44 Rumelhart, D.E., Hinton, G.E., Williams, R.J.: 'Learning representations by back-propagating errors' *Nature*, 1986, **323**, (6088), pp. 533–536.

45 Box, G.E.P., Pierce, D.A.: 'Distribution of residual autocorrelations in autoregressive-integrated moving average time series models' *J. Am. Stat. Assoc.*, 1970, **65**, (332), pp. 1509–1526.

46 Chollet, F.: 'Keras: the Python deep learning API' (2015)

47 Abadi, M., Agarwal, A., Barham, P., *et al.*: 'TensorFlow: Large-Scale Machine Learning on Heterogeneous Distributed Systems' (2015)

48 H2O.ai: 'H2O AutoML' (2017)

49 Smith, T.G.: 'pmdarima: ARIMA estimators for Python' (2017)